Click Here for Full Article

Modulation of the aerosol absorption and single-scattering albedo due to synoptic scale and sea breeze circulations: United Arab Emirates experiment perspective

J. Remiszewska,[1] P. J. Flatau,[2] K. M. Markowicz,[3] E. A. Reid,[4] J. S. Reid,[4] and M. L. Witek[3]

[1]   The spectral aerosol absorption properties in the Arabian Gulf region were observed during the United Arab Emirates Unified Aerosol Experiment (UAE^2). Measurements were taken at a coastal region of the Arabian Gulf located 60 km northeast of Abu Dhabi, the capital of the United Arab Emirates, allowing characterization of pollution and dust absorption properties in a highly heterogeneous environment. A large observed change of the diurnal signal during the period under study (27 August through 30 September 2004) was due to (1) strong sea and land breeze and (2) changes in prevailing synoptic-scale flow. During the night, stagnating air resulted in gradual accumulation of pollution with maximum absorption in the early morning hours. The rising sun increased both the depth of the boundary layer and the temperature of the interior desert, resulting in strong and sudden sea breeze onset which ventilated the polluted air accumulated during the night. Our observations show that the onshore winds brought cleaner air resulting in decreasing values of the absorption coefficient and increasing values of the single-scattering albedo (SSA). The mean value of the absorption coefficient at 550 nm measured during the sea breeze was 10.2 ± 0.9 Mm^{-1}, while during the land breeze it was 13.8 ± 1.2 Mm^{-1}. Synoptic-scale transport also strongly influenced particle fine/coarse partition with "northern" flow bringing pollution particles and "southern" flow bringing more dust.

1.   Introduction

[2]   The importance of aerosol light absorption in the atmosphere's radiative budget as well as in satellite retrievals is universally recognized. Despite this, a great deal of disagreement occurs within the scientific community. For example, consider airborne dust. Optical properties of dust have been studied extensively using remote sensing [*Alpert and Ganor*, 2001; *Kalashnikova et al.*, 2005; *Reid et al.*, 2003; *Tanré et al.*, 2003] and in situ measurements [*Haywood et al.*, 2001; *Tanré et al.*, 2003]. In general, there is considerable divergence between these methods, with reported single-scattering albedo values at 550 nm for dust ranging from 0.888 [*Hess et al.*, 1998] to 0.99 [*Haywood et al.*, 2003].

[3]   There are a number of reasons why such divergence occurs, including in situ absorption methodologies that have been repeatedly questioned [*Bond and Bergstrom*, 2006]. In order to reconcile these questions, a consistent set of measurements needs to be made in which the influence of physical parameters on the system can be studied along with response of the individual methods. For example, one would want to compare periods dominated by coarse mode particles with fine mode dominated conditions. Changing particle chemistries would also be beneficial, and humidity impacts need to be characterized. All of these conditions are met in Southwest Asia, where researchers can take advantage of varying regional aerosols driven by the physical meteorology.

[4]   The region surrounding the Arabian Gulf has recently been identified as the world's third largest dust source [*Léon and Legrand*, 2003], having maximum dust source activity during the spring and summer. The Arabian Gulf provides a unique laboratory to study the properties of dust and, as this region is a large source of anthropogenic emissions [*Langner et al.*, 1992], dust's interaction with pollution can also be investigated. Mostly local refineries, factories and fossil fuel combustion, emit atmospheric pollutants though there is also significant transport from the Indian

[1]Institute of Geophysics, Polish Academy of Sciences, Warszawa, Poland.
[2]Scripps Institution of Oceanography, University of California San Diego, San Diego, California, USA.
[3]Institute of Geophysics, Warsaw University, Warszawa, Poland.
[4]Naval Research Laboratory, Marine Meteorology Division, Monterey, California, USA.

subcontinent. The concentration of aerosols depends on many factors including meteorological conditions [*Léon and Legrand*, 2003] and atmospheric circulation [*Li and Ramanathan*, 2002].

[5] Despite the uniqueness of the region, the aerosol optical properties in the Arabian Gulf region are not well characterized. Previous ground and airborne measurements were made in the spring and summer of 1991 [*Draxler et al.*, 1994; *Hobbs and Radke*, 1992; *Nakajima et al.*, 1996] and were focused on the Kuwait oil fires. To our knowledge, the only published study of background conditions of aerosol optical properties in the region utilized direct sun and sky scanning radiometers [*Smirnov et al.*, 2002] and presented spectral dependency of the single-scattering albedo (SSA) for dusty and nondusty conditions.

[6] Because the Arabian Gulf region's atmosphere is conducive to investigation of the fidelity of remote sensing systems, the United Arab Emirates (UAE) Unified Aerosol Experiment (UAE^2) was performed. Conducted in August and September of 2004, UAE^2 included a comprehensive calibration and validation component to study the impact of dust absorption on space and surface based remote sensing retrievals over dark and bright surfaces. Two surface atmospheric research supersites and fifteen Aerosol Robotic Network Sun Photometers (AERONET) sites were deployed in coastal and desert regions of the UAE. One of the two surface stations, the Naval Research Laboratory's Mobile Atmosphere, Aerosol and Radiation Characterization Observatory (MAARCO) was located on the Arabian Gulf coast approximately 60 km northeast of Abu Dhabi, away from the primary city plume. This location allowed studies of aerosol properties over coastal desert as characterized by the strong sea and land breeze circulations. These intense local circulations are a regular phenomenon in the coastal region of the Arabian Gulf, in the absence of strong mesoscale flow [*Zhu and Atkinson*, 2004]. The onshore sea breeze develops about 1300 local time (LT) (0900 UTC) and lasts till 2400 LT (1800 UTC), and is always associated with both an abrupt change of the wind direction and increased wind strength, in comparison to the land breeze. Winds associated with the sea breeze over the UAE coastline come mostly from the north with maximum velocities reaching values of about 6 ms^{-1} [*Zhu and Atkinson*, 2004], a value typical for a well developed moderate sea breeze [*Miller et al.*, 2003]. During the night, the land breeze is characterized by low wind speeds of about 3 ms^{-1}.

[7] The purpose of this study is to extend previous knowledge and present the absorption coefficients and single-scattering albedo measured in the coastal region of the Arabian Gulf [*Draxler et al.*, 1994; *Hobbs and Radke*, 1992; *Nakajima et al.*, 1996; *Smirnov et al.*, 2002]. This will provide baseline absorption data for many subsequent manuscripts that will examine aerosol particle properties and remote sensing algorithm fidelity. The results are based on the data collected during several weeks of measurements performed at the MAARCO facility.

2. Instruments and Methods

[8] In this section we describe instrumentation and describe methods for derivation of the absorption coefficient and the atmospheric single-scattering albedo.

2.1. Scattering Coefficient

[9] The aerosol scattering (σ_{scat}) and the hemispheric backscattering coefficients (σ_{bscat}) were measured by a TSI 3563 nephelometer at three wavelengths: 450, 550, 700 nm. The instrument detects total scattered light between $7-170$ degrees and corrections are applied to get the aerosol scattering by subtracting light scattered by the air molecules, the instrument walls, the detector background noise, and by reducing the results to $0-180$ degrees range [*Anderson et al.*, 1996; *Heintzenberg and Charlson*, 1996]. During the experiment two nephelometers were simultaneously operated; one at near-atmospheric conditions and the other one at constant relative humidity of about 35%.

[10] Air was sampled from a total suspended particulate matter (TSP) inlet that fed the in situ aerosol instruments. Consequently, the instruments measured fine and coarse mode simultaneously. To separate the contributions, often it is assumed that the scattering σ_{scat} is given by the following power law

$$\sigma_{\text{scat}} = \beta \lambda^{-\alpha}, \tag{1}$$

where Ångstrom coefficient α is given by

$$\alpha_{neph} = \frac{-\log\left(\dfrac{\sigma_{scat,450}}{\sigma_{scat,700}}\right)}{\log\left(\dfrac{450}{700}\right)}, \tag{2}$$

and $\sigma_{\text{scat},450}$, $\sigma_{\text{scat},700}$ are scattering coefficients at 450 nm and 700 nm.

[11] In general, α increases with the decreasing particle size and is smaller when large mode particles are dominating the size distribution.
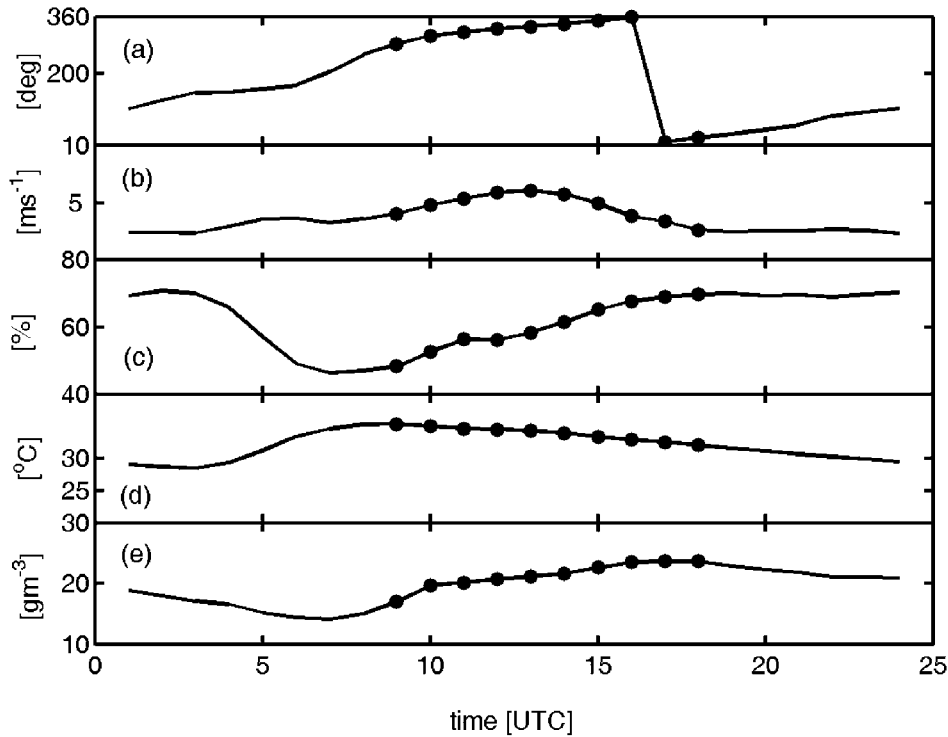
2.2. Absorption Coefficient

[12] The absorption coefficient was derived from Magee Scientifc aethalometer (AE30) measurements. This instrument is designed for real-time continuous measurements of black carbon aerosol particle concentration [*Hansen et al.*, 1996]. The aethalometer continuously draws air samples through the inlet port, depositing the aerosols on a fibrous filter media while performing continuous optical measurements of that filter media. Two detectors monitor the light transmission through the filter; one measures the light beam attenuation through the sample and filter and the other measures the light passing through a clean, reference filter section. The aethalometer measures the transmission through the filter over the wide spectrum of wavelengths, in our case 370, 430, 470, 520, 590, 700, 880 nm, and computes and reports the aerosol mass concentration [ng m^{-3}].

[13] The absorption coefficient (σ_{abs}) is related to light intensity attenuation via Beer's law

$$I = I_0 e^{-\sigma_{abs}\Delta z}, \tag{3}$$

where I_0 is the intensity of the incoming light and I is the intensity of attenuated light. The light beam attenuation reported by the aethalometer is defined as

$$ATN = \ln(I/I_0). \tag{4}$$

Figure 1. Mean diurnal cycle of (a) wind direction, (b) wind speed, (c) relative humidity, (d) temperature, and (e) absolute humidity. Solid circles indicate sea breeze.

[14] For the reported mass of black carbon one can calculate the aerosol absorption coefficient of the particles deposited on the filter by multiplying by the specific cross section for absorption of the black carbon (BC). Specific absorption of black carbon, reported by literature, varies in range depending on its properties from 2 to 25 $m^2 g^{-1}$ [*Barnard et al.*, 2005; *Petzold et al.*, 1997]. Another way to calculate the absorption coefficient σ_{aeth} is to consider change of attenuation during the time interval d*ATN*/dt [*Arnott et al.*, 2005; *Fialho et al.*, 2005]. This leads to

$$\sigma_{aeth} \equiv \frac{A}{V} \frac{dATN}{dt}, \tag{5}$$

where A is the aerosol spot area and V is the flow rate.

[15] However, σ_{aeth} is influenced by the filter and scattering by the collected aerosol particles and hence needs correction for these contributions [*Weingartner et al.*, 2003]. A two-stream approximation methodology, which considers both filter and aerosol layers, was recently developed by [*Arnott et al.*, 2005]. These authors provide information about the optical reflectance and transmission of the filter used in the aethalometer.

[16] Our approach relies on the two-stream approximation described by [*Bohren*, 1987] and [*Arnott et al.*, 2005]. In short, we use an iterative method to match measured attenuation with attenuation predicted from the two-layer system in the two-stream approximation. In this method the only unknown quantity is the absorption coefficient. We should mention that there exist noniterative methods, which convert σ_{aeth} to absorption coefficient by introducing

semiempirical coefficients to account for filter scattering [*Weingartner et al.*, 2003].

[17] From absorption and scattering coefficients we can compute the single-scattering albedo ω_o defined as:

$$\omega_o = \frac{\sigma_{scat}}{\sigma_{scat} + \sigma_{abs}}. \tag{6}$$

2.3. Other Data

[18] We used the Hybrid Single-Particle Lagrangian Integrated Trajectory (HYSPLIT) model [*Draxler and Hess*, 1998] to compute 72 hours backward trajectories for the MAARCO location (24.7°N, 54.7°E). The HYSPLIT model is a complete system for computing air parcel trajectories at different levels. We used HYSPLIT to compute trajectories at 10, 500, and 1000 meters above the ground to detect synoptic-scale air mass trajectories. The meteorological data are based on the NCEP Global Forecast System data with an assimilation system cycle of 6 hours and resolution 1×1 degree.

[19] Bulk fine/coarse mass concentrations were also used. 47 mm filters were sampled for 24 hours each day (~0930 local time change out). From these PM2.5 and TSP mass concentrations were derived.

3. Meteorological Summary

3.1. Diurnal Cycle

[20] In this section we present daily changes of the aerosol optical properties in relation to land and sea breeze development. We concentrate on the mean diurnal cycle of
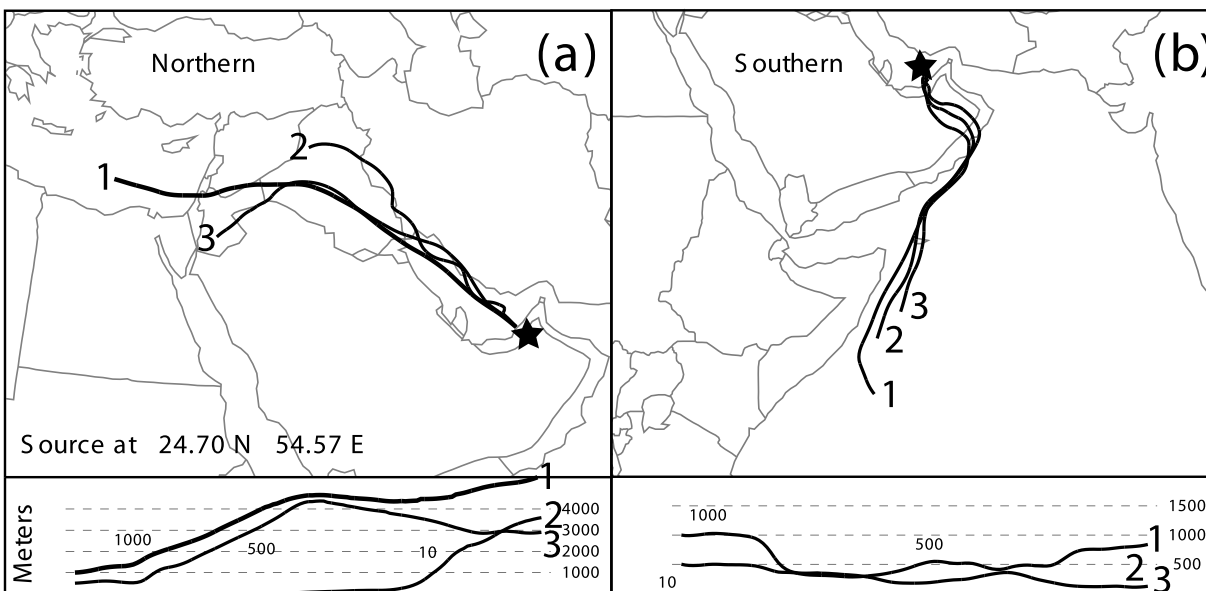
Figure 2. Examples of backward trajectories computed for the Naval Research Laboratory's Mobile Atmosphere, Aerosol and Radiation Characterization Observatory (MAARCO) location at three levels: 10 m (line 2), 500 m (line 3), and 1000 m (line 1) by the Hybrid Single-Particle Lagrangian Integrated Trajectory (HYSPLIT) model. On this basis we distinguish two types of synoptic airflow: (a) northern and (b) southern.

the absorption coefficient, the single-scattering albedo, and relevant diurnal meteorological conditions. Sea breeze is defined in terms of the wind direction; winds from 270 to 30 degrees define sea breeze and winds from 30 to 270 degrees define land breeze.

[21] Figure 1 shows mean diurnal cycle of the wind direction (Figure 1a), wind speed (Figure 1b), relative humidity (Figure 1c), temperature (Figure 1d) and absolute humidity (Figure 1e). On these figures, dots indicate the sea breeze conditions. The data were collected from 1–22 September 2004. Solid lines are 1-hourly averages. Figure 1a indicates that the diurnal change of wind direction is clockwise with fairly rapid sea breeze onset at around 0900 UTC. One should be aware that these plots are averaged over approximately 1 month. In reality, values of meteorological fields are more abrupt than those presented in this section. It can be seen (Figure 1a) that on average the sea breeze duration is from 0900 UTC to 1800 UTC. The mean surface wind speed (Figure 1b) during land breeze remains in the range of $1-3$ ms^{-1}. From 0300 UTC winds are gradually increasing until they reach the maximum of 6.0 ms^{-1} at 1300 UTC and gradually decrease to 2.5 ms^{-1} at 1900 UTC; after which they remain constant. It is evident that the largest values of wind speed are associated with the sea breeze cycle. Figures 1c and 1d present mean diurnal cycle of relative humidity (RH) and temperature, respectively. It is apparent that the diurnal cycle of RH is controlled by the solar insolation and corresponding surface temperature changes. The RH changes are inversely proportional to the mean surface temperature trend. The mean RH decreases gradually from 70% to less then 50% between 0100–0600 UTC. After the sea breeze onset RH increases gradually to 70% at the end of the day. Mean temperature varies from 30°C to 34°C. It reaches maximum value at

0800 UTC (1200 LT). The diurnal cycle of absolute humidity is presented in Figure 1e. The rapid increase starts in the morning at 0600 UTC ending with the maximum value of about 23 g m^{-3} at 1800 UTC. This corresponds to both increased surface temperature and flow onset from the Arabian Gulf. Beginning 0800 UTC this trend reverses. Thus it is observed that increased specific humidity correlates well with the duration of the sea breeze.

3.2. Synoptic Back Trajectories and Synoptic-Scale Influence of Sea and Land Breeze

[22] Synoptic back trajectories computed by the HYSPLIT model (Figure 2) show the MAARCO location was influenced by the synoptic-scale air mass flow which we approximate as (1) north (33% of all cases), (2) south (47%), and (3) "mixed" direction (20%).

[23] Figure 2a illustrates the "north" trajectories for September 2004. Similarly, "south" flow is illustrated in Figure 2b. The rest of cases (20%) can't be clearly classified into north or south category and we call these "mixed" flows. The mean meteorological conditions of temperature and wind speed do not change considerably from the pattern described above. Figure 3 presents the mean diurnal cycles of absolute humidity for each type of flow. It is apparent that the air masses traveling across the Gulf carry more moist air than the ones traveling across the land. The magnitude of the diurnal change of the absolute humidity is largest for the southern flow cases.

4. Results

4.1. Diurnal Cycle of the Aerosol Optical Properties

[24] In this section we present daily changes of the aerosol optical properties in relation to land and sea breeze onset. The time series of absorption coefficients and atmo-
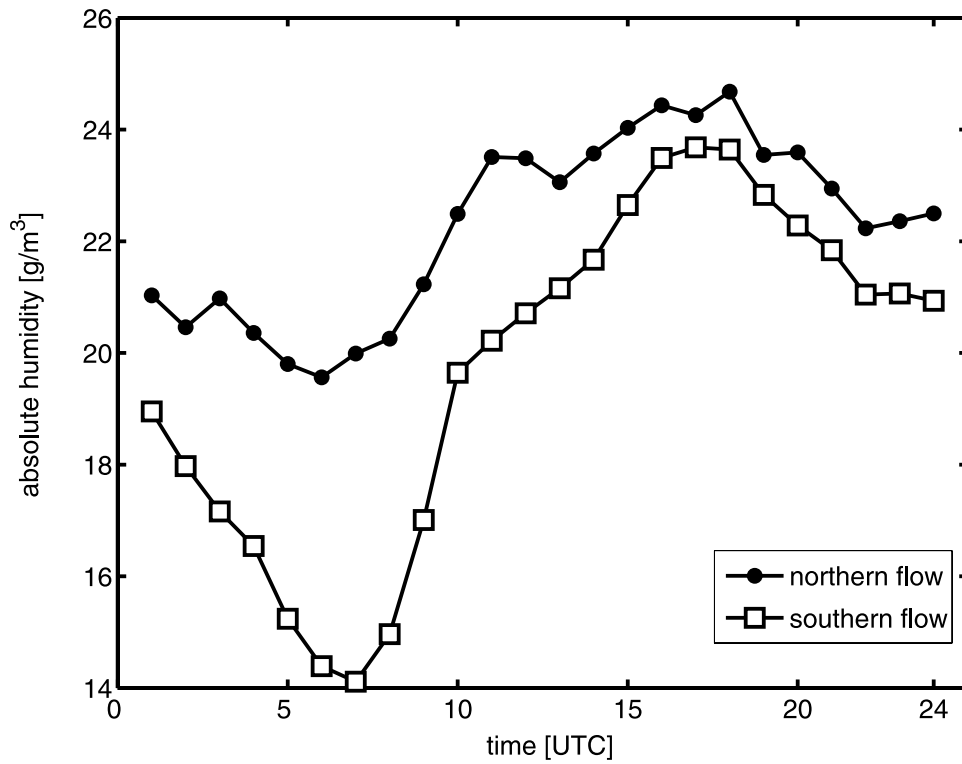
**Figure 3.** Mean diurnal cycle of absolute humidity for northern and southern flow.

spheric single-scattering albedo are presented in Figure 4. The data were collected over the period of time from 27 August to 30 September 2004 and averaged in 1-hour bins. Characteristic regular minima in absorption coefficient values and respectively maxima in SSA are apparent. The diurnal variability of these quantities is discussed later.

[25] In order to examine the wavelength dependence of SSA we introduce the Ångstrom-like coefficient defined for
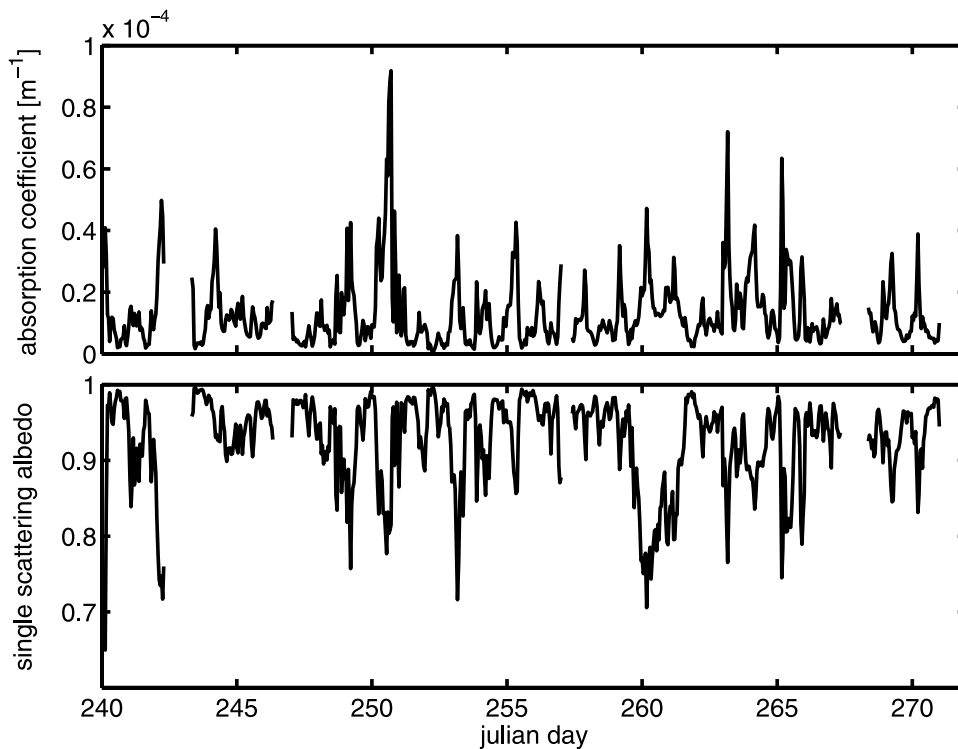
Figure 4. Time series of the absorption coefficient and single-scattering albedo at 550 nm from 27 August to 30 September 2004. Data were averaged in 1-hour bins.
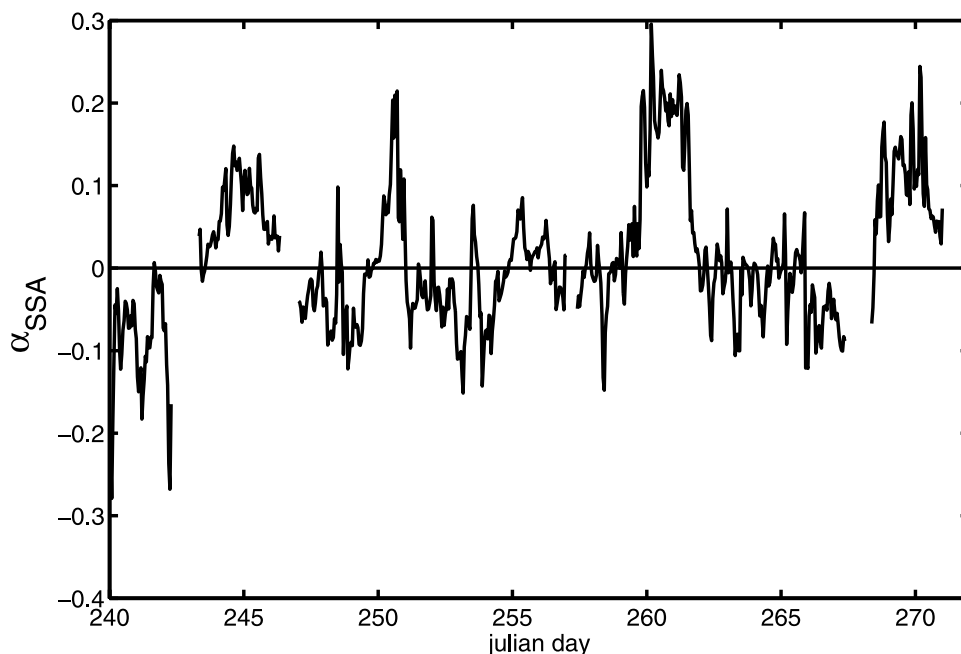
Figure 5. Ångstrom coefficient for single-scattering albedo averaged in 1-hour bins.
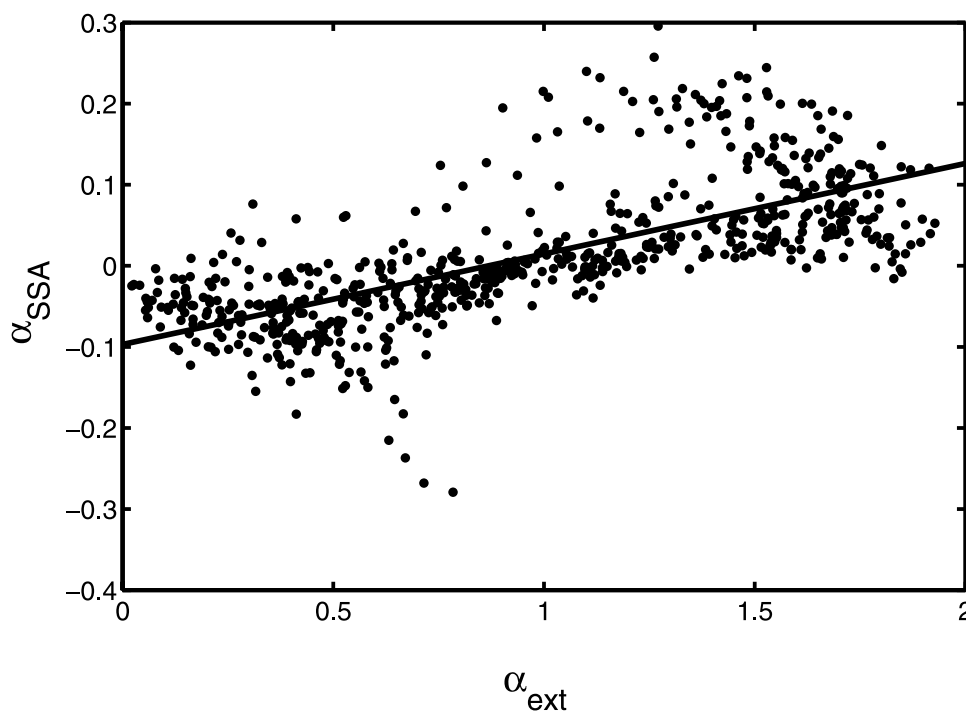
the single-scattering albedo at 450 nm and 700 nm. It is given by:

$$\alpha_{SSA} = \frac{-\log\left(\frac{\omega_{450}}{\omega_{700}}\right)}{\log\left(\frac{450}{700}\right)}, \quad (7)$$

where ω_{450}, ω_{700} denote single-scattering albedo at 450 nm and 700 nm. If α_{SSA} is less than 0 it indicates that SSA increases with wavelength, while if α_{SSA} is larger than 0, SSA decreases with wavelength. Figure 5 presents time series of α_{SSA} from 27 August to 30 September 2004. Clearly, wavelength dependency changes during the measurement time. We observe a few episodes when SSA decreases with the wavelength as well as a few episodes when SSA increases with the wavelength.

[26] Figure 6 presents relationship between the Ångstrom coefficient defined for the SSA (α_{SSA}) and extinction (α_{ext}). Overall, the spectral wavelength dependence of SSA

Figure 6. Extinction versus single-scattering albedo Ångstrom coefficient.
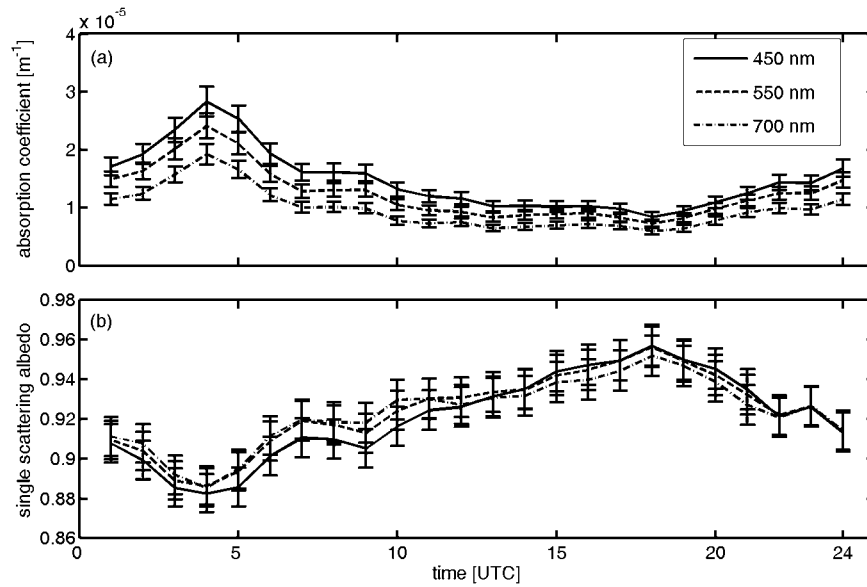
Figure 7. Diurnal cycle of (a) the absorption coefficient and (b) atmospheric single-scattering albedo at three wavelengths: 450 nm, 550 nm, and 700 nm. Data were collected and averaged from 27 August to 30 September 2004.

changes its behavior between fine and coarse mode particles. For small particles this dependence follows λ^{-b}, while for Ångstrom coefficient for extinction less than unity, the SSA dependence is λ^{b}, where b is a positive exponent.

[27] The mean diurnal cycles of the absorption coefficient and single-scattering albedo are presented in Figure 7. These data were averaged over the period from 27 August 2004 to 30 September 2004 in 1-hour bins. The absorption coefficient (Figure 7a) is at maximum in the early morning at around 0400 UTC because of weak winds and stable conditions. The absorption coefficient gradually decreases from about 2.4×10^{-5} m^{-1} at 550 nm to about 0.7×10^{-5} m^{-1}, reaching minimum values between 1000 UTC and 2000 UTC. This is associated with the sea breeze development and its ventilating effect. From about 1800 UTC there is a gradual absorption increase which is related to wind shift and transport of pollution from land.

[28] The diurnal cycle of atmospheric single-scattering albedo is presented in Figure 7b. Its behavior strongly depends on absorption coefficient. The developing sea breeze results in an increase of SSA values between 0900 UTC and 1800 UTC. It reaches maximum of about 0.95 for the 550 nm channel at 1800 UTC, the time at which the absorption coefficient reaches minimum. The minimum value of the SSA is 0.88 at 550 nm at 0400 UTC and corresponds to the maximum value of the absorption

coefficient. Table 1 presents mean values of the absorption coefficient and the atmospheric single-scattering albedo during the sea and land breeze and mean values of these quantities averaged over the period from 27 August 2004 to 30 September 2004.

[29] Mean values of the absorption coefficient follow the pattern described above with smaller absorption coefficient and larger SSA during the sea breeze, and larger absorption coefficient with smaller atmospheric SSA values during the land breeze. Mean values of the atmospheric single-scattering albedo are similar in all channels. However, Figure 7b indicates that during the sea breeze there is an increasing atmospheric SSA trend.

[30] Looking at the atmospheric SSA and absorption coefficient quantitatively we notice (not shown) that almost 75% of all cases correspond to the absorption coefficient with values below 20 Mm^{-1}. Almost 80% of all cases correspond to values of SSA above 0.9.

[31] Figure 8 presents mean diurnal cycle of the Ångstrom coefficient ($\alpha_{450-700\ nm}$). It increases from 0.8 to 1.1 as the sea breeze develops. Thus during the sea breeze the fraction of small particles is gradually increasing. Anticipating that this fraction may be related to soot and other anthropogenic aerosol particles, we now examine spectral dependence of SSA for soot, water soluble aerosol, and dust. Water soluble aerosol class is often used to describe anthropogenic aerosols [Hess et al., 1998].

Table 1. Mean Values of the Absorption Coefficient at 450, 550, and 700 nm Averaged Over the Period From 27 August to 30 September 2004 ($\sigma_{abs,mean}$) for the Sea Breeze $\sigma_{abs,sea\ breeze}$, and for the Land Breeze $\sigma_{abs,land\ breeze}$[a]

| Wavelength, nm	$\sigma_{abs,mean}$, Mm^{-1}	$\sigma_{abs,sea\ breeze}$, Mm^{-1}	$\sigma_{abs,\ land\ breeze}$, Mm^{-1}	ω_{mean}	$\omega_{sea\ breeze}$	$\omega_{land\ breeze}$
450	15.0 ± 1.4	11.2 ± 1.0	17.4 ± 1.6	0.92 ± 0.01	0.93 ± 0.01	0.91 ± 0.01
550	12.0 ± 1.1	10.2 ± 0.9	13.8 ± 1.2	0.92 ± 0.01	0.93 ± 0.01	0.91 ± 0.01
700	10.0 ± 0.9	7.3 ± 0.7	11.6 ± 1.0	0.92 ± 0.01	0.93 ± 0.01	0.91 ± 0.01

[a]Also presented are the SSA values. Errors are calculated by applying the first-order approximation of error propagation theory.
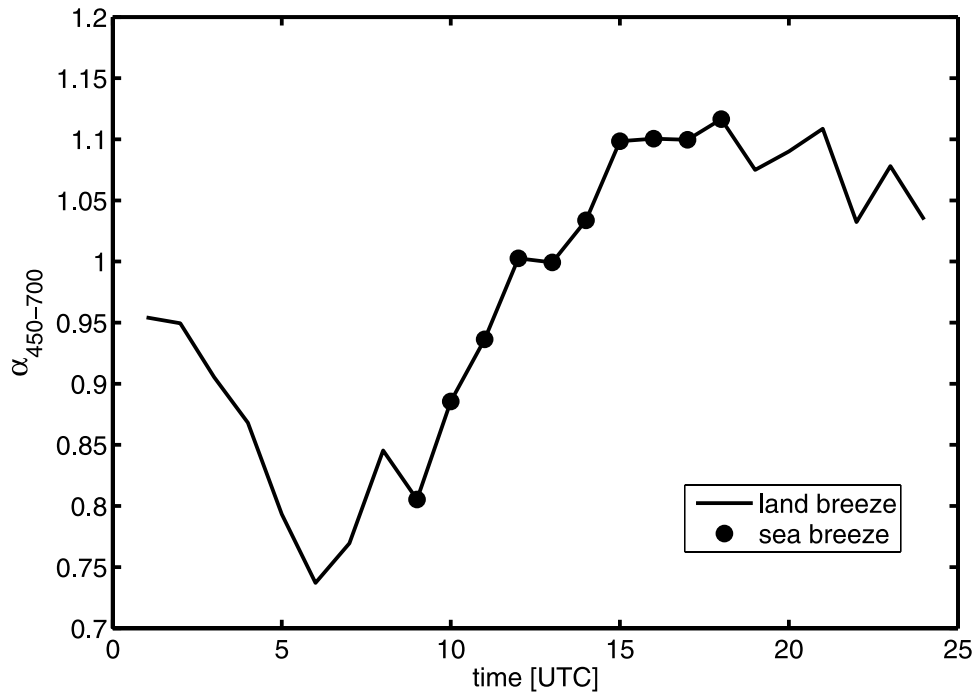
Figure 8. Diurnal cycle of the Ångstrom coefficient averaged from 27 August 2004 to 30 September 2004 in 1-hour bins.

[32] Figure 9 shows spectral dependence of the SSA for soot (Figure 9a), water soluble aerosol (Figure 9b), and dust particles (Figure 9c) based on the online public access catalog (OPAC) database. One can observe that for soot and water soluble aerosol the SSA values decreases as wavelength increases. Therefore we hypothesize that the change in spectral dependence of SSA is due to presence of
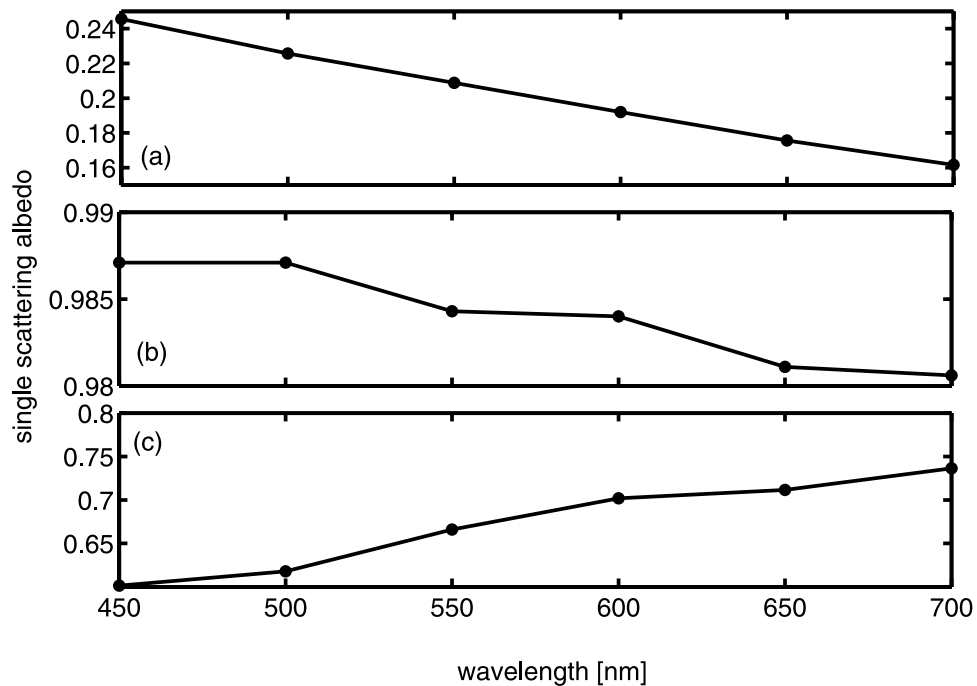
Figure 9. Wavelength dependency of SSA for (a) soot, (b) water soluble aerosols, and (c) coarse mode dust particles based on the online public access catalog (OPAC) database.
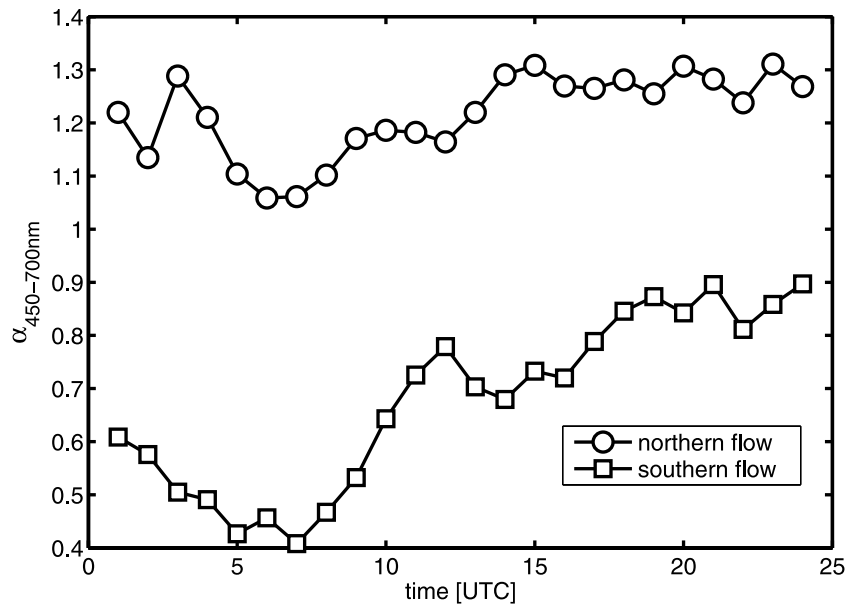
Figure 10. Mean diurnal cycle of the Ångstrom coefficient based on 450 and 700 nm nephelometer channels for northern and southern synoptic flow.

small mode soot and water soluble particles. These kind of aerosols are characteristic for urban and industrial areas.

4.2. Synoptic-Scale Flow and Local Sea Breeze Effects

[33] Previous analysis focused on the local circulation and its influence on the aerosol optical properties. We will now discuss synoptic-scale circulation impact on aerosol optical properties. As was discussed in the "Meteorological Summary" section we can distinguish three synoptic-scale regimes in the region: (1) flow from the north (33% of all cases), (2) south (47%), and (3) "mixed" flow.

[34] Figure 10 presents mean diurnal cycle of the Ångstrom exponent ($\alpha_{450-700\ nm}$) for two major types of
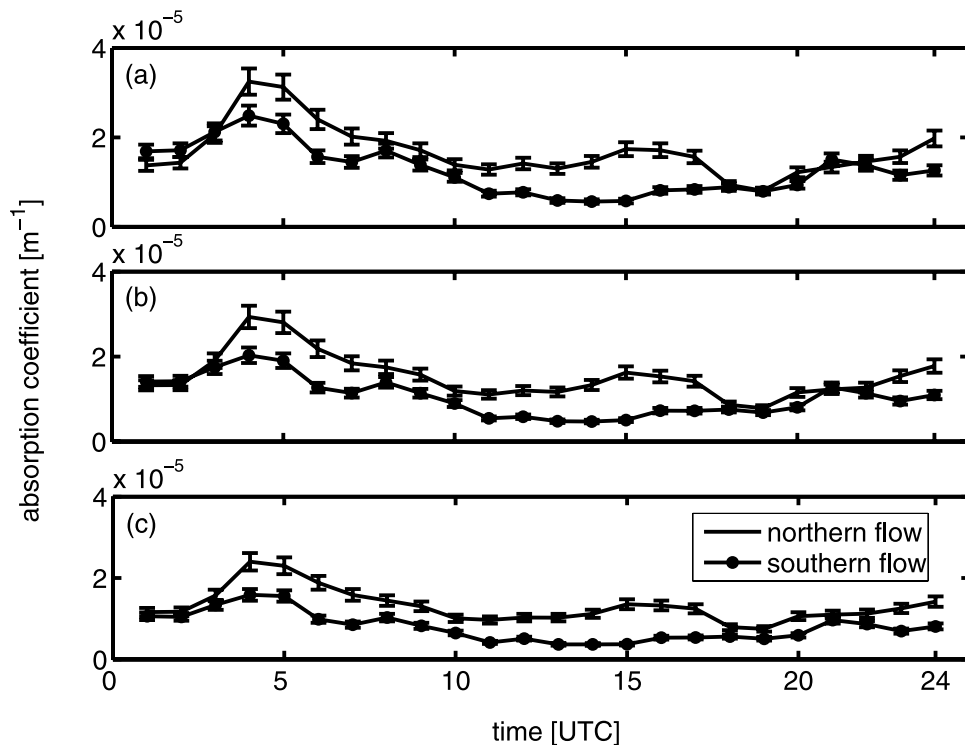
Figure 11. Mean diurnal cycle of the absorption coefficient for northern and southern synoptic flows for (a) 450 nm, (b) 550 nm, and (c) 700 nm.

Table 2. Mean Values of the Absorption Coefficient (σ_{abs}) at 450, 550, and 700 nm for Northern, Southern, and "Mixed" Flows[a]

Wavelength, nm	σ_{abs}, Mm^{-1}		
	Northern Flow	Southern Flow	"Mixed" Flow
450	16.4 ± 1.5	12.2 ± 1.1	16.5 ± 1.5
550	14.9 ± 1.3	10.1 ± 0.9	14.1 ± 1.3
700	12.7 ± 1.1	7.6 ± 0.7	10.7 ± 1.0

[a]Errors are calculated by applying the first-order approximation of error propagation theory.

Table 3. Mean Values of Absorption Coefficient During Sea Breeze ($\sigma_{abs,sea\ breeze}$) and Land Breeze ($\sigma_{abs,land\ breeze}$) for Northern and Southern Flow[a]

Wavelength, nm	$\sigma_{abs,sea\ breeze}$, Mm^{-1}		$\sigma_{abs,land\ breeze}$, Mm^{-1}	
	Northern Flow	Southern Flow	Northern Flow	Southern Flow
450	14.5 ± 1.3	9.1 ± 0.8	19.2 ± 1.7	14.2 ± 1.3
550	13.2 ± 1.2	7.7 ± 0.7	17.4 ± 1.6	11.7 ± 1.1
700	11.4 ± 1.0	5.9 ± 0.6	14.8 ± 1.3	8.7 ± 0.8

[a]Errors are calculated by applying the first-order approximation of error propagation theory.

flow. It is apparent that the aerosol origin is an important factor determining the size of particles. The northern flow carries more fine particles – Ångstrom exponent exceeds unity with a mean value of 1.22. The southern flow is dominated by larger particles with mean value of Ångstrom exponent of 0.68.

[35] Figure 11 presents mean diurnal cycles of absorption coefficient at 450, 550, 700 nm for two synoptic-scale cases. Table 2 summarizes the mean values of absorption coefficient for northern, southern, and "mixed" flows. It is apparent that northern flow carries more absorptive aerosol than the southern one.

[36] Table 3 provides information about the influence of the sea-land breeze circulation on the value of the absorption coefficient. Mean values of absorption coefficients during the sea breeze are about 2 times less for the southern flow than for the northern, which is related to smaller anthropogenic aerosol possibly coming from Kuwait or Iraq; while the southern flow brings more dust particles from the deserts in UAE, Oman and Saudi Arabia. This hypothesis is confirmed by the diurnal cycles of SSA.

[37] Figure 12 presents the diurnal cycle of atmospheric SSA in blue, green, and red channels for two types of flow. The atmospheric single-scattering albedo is greater for southern flow than for northern and the difference becomes greater as the sea breeze develops. Similar results are seen for the absorption coefficient in Figure 13.

[38] We see that atmospheric single-scattering albedo decreases with wavelength for aerosols transported from the north and increases when aerosols come from the south (dust). The wavelength dependency of the atmospheric SSA for the northern flow presented in Figure 12 is characteristic of industrial aerosol [Dubovik et al., 2002]. It is also consistent with the larger values of the absorption coefficient in comparison to the values observed for the southern flow.

[39] It is clear from Figure 12 that change from smaller values of the atmospheric SSA to larger values during the sea breeze is more rapid for the southern flow. This is because the prevailing cleaner southern flow is interacting
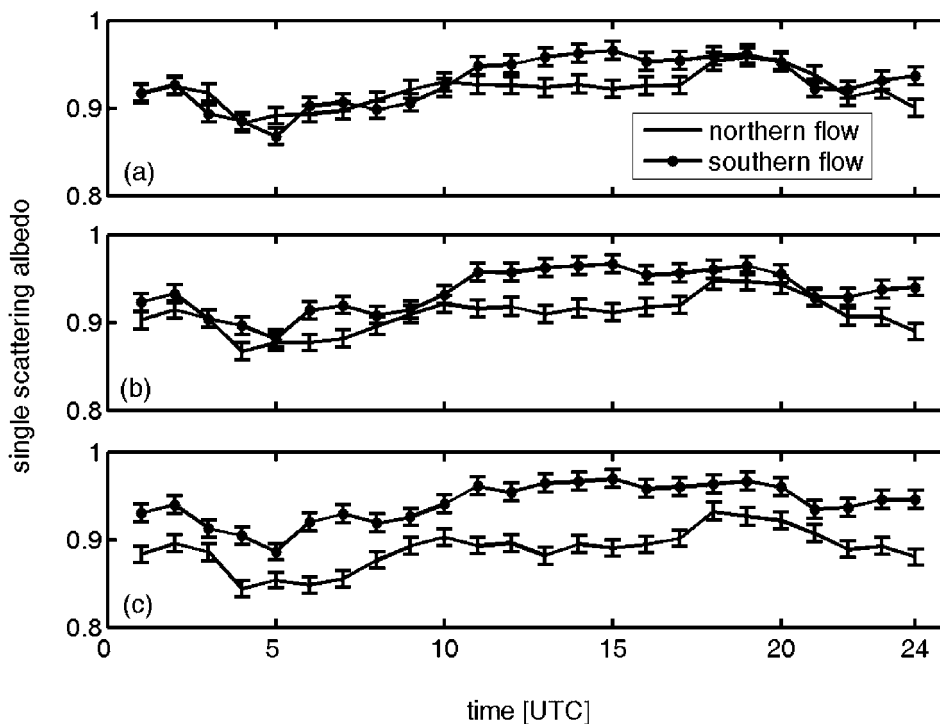
Figure 12. Mean diurnal cycle of the atmospheric single-scattering albedo for northern and southern synoptic flow at (a) 450 nm, (b) 550 nm, and (c) 700 nm.
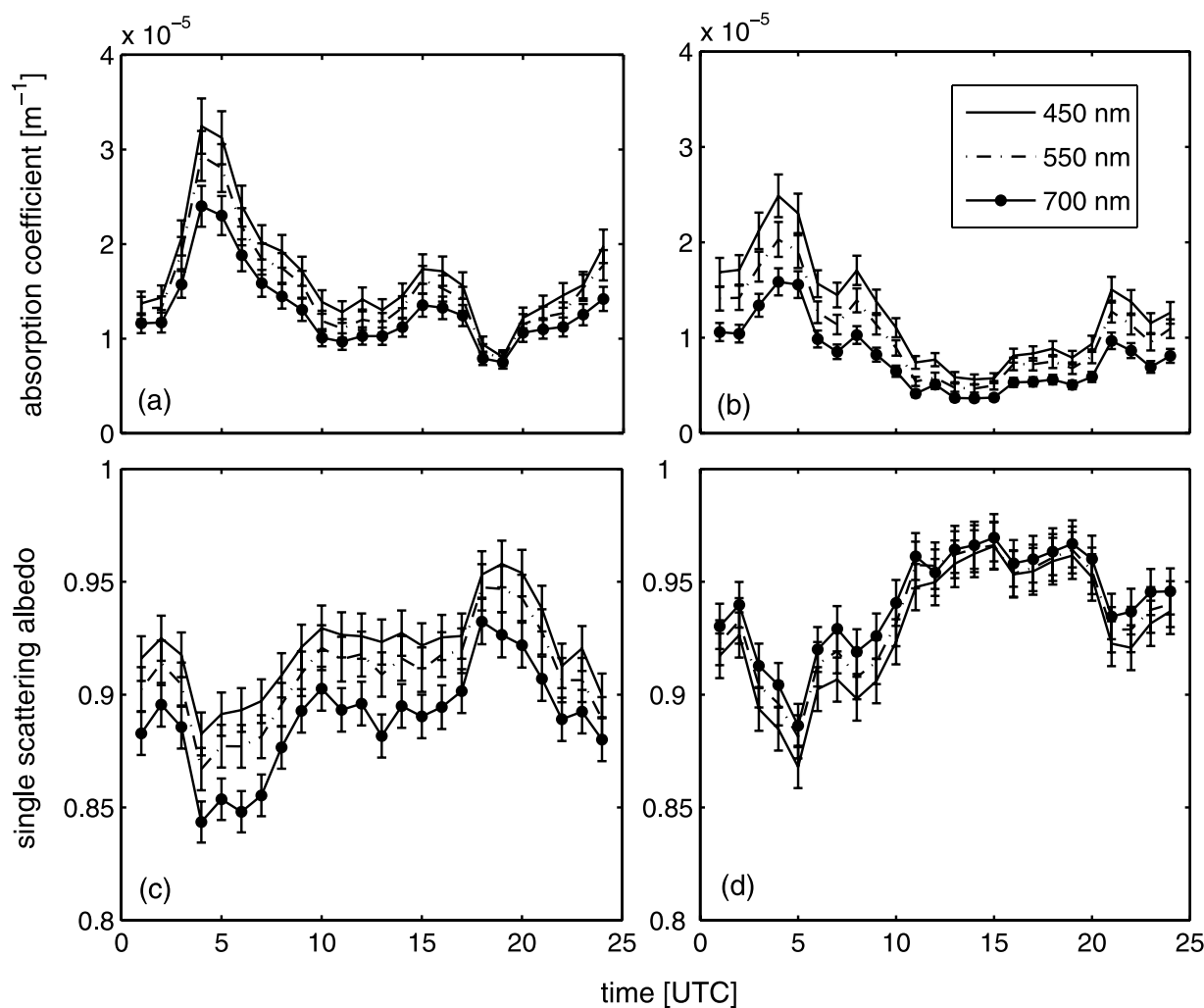
Figure 13. Mean diurnal cycle of the absorption coefficient at 450 nm, 550 nm, and 700 nm for (a) northern flow and (b) southern flow and mean diurnal cycle of the atmospheric single-scattering albedo for (c) northern and (d) southern synoptic flow.

with the onshore winds. Sea breeze lasts from 0900 UTC to 1700 UTC and during this time we observe an increasing trend of the atmospheric SSA values from 0.91 at 550 nm to about 0.96 during the well-developed sea breeze. On the other hand, when air moves from the north carrying in industrial pollution, we observe a slight increase of the atmospheric SSA values from 0400 UTC to 1900 UTC.

[40] Distribution of the atmospheric SSA at 550 nm (not presented) shows, that during the sea breeze and northern flow there is significant contribution (35%) of SSA values below 0.9 but there are only 10% of such cases for the southern flow. Values of SSA above 0.9 constitute 90% of all cases for the southern flow and about 65% for the northern flow.

5. Summary

[41] In the summer of 2004 the coastal region of the Arabian Gulf northeast of Abu Dhabi, the capital of the United Arab Emirates, was influenced by synoptic-scale circulation, characterized by very intense land and sea breeze circulation. The atmospheric aerosol single-scattering properties were strongly influenced by the synoptic-scale and local-scale systems. During the night, the stagnating air results in gradual accumulation of pollution with maximum absorption in the early morning hours. The rising sun increases the depth of the boundary layer and increases temperature of the interior desert. This results in strong and sudden sea breeze onset that ventilates polluted air accumulated during the night. However, the air over the Arabian Gulf and its surroundings is itself polluted, which we document on the basis of absorption and scattering measurements. In particular, the "northern" flow brings smaller particles and the "southern" flow brings air with larger particles from dusty regions. A simplified diagrammatic representation of the interaction between the synoptic-scale airflow information and the local sea and land breeze here discussed, is presented in Figure 14.

[42] Mean value of the absorption coefficient at 550 nm during the land breeze is 35% higher than during the sea breeze case. The atmospheric single-scattering albedo increases during the sea breeze reaching a maximum value of about 0.95 in the 550 nm channel at 1900 UTC. The 72-hour back trajectories computed using the HYSPLIT
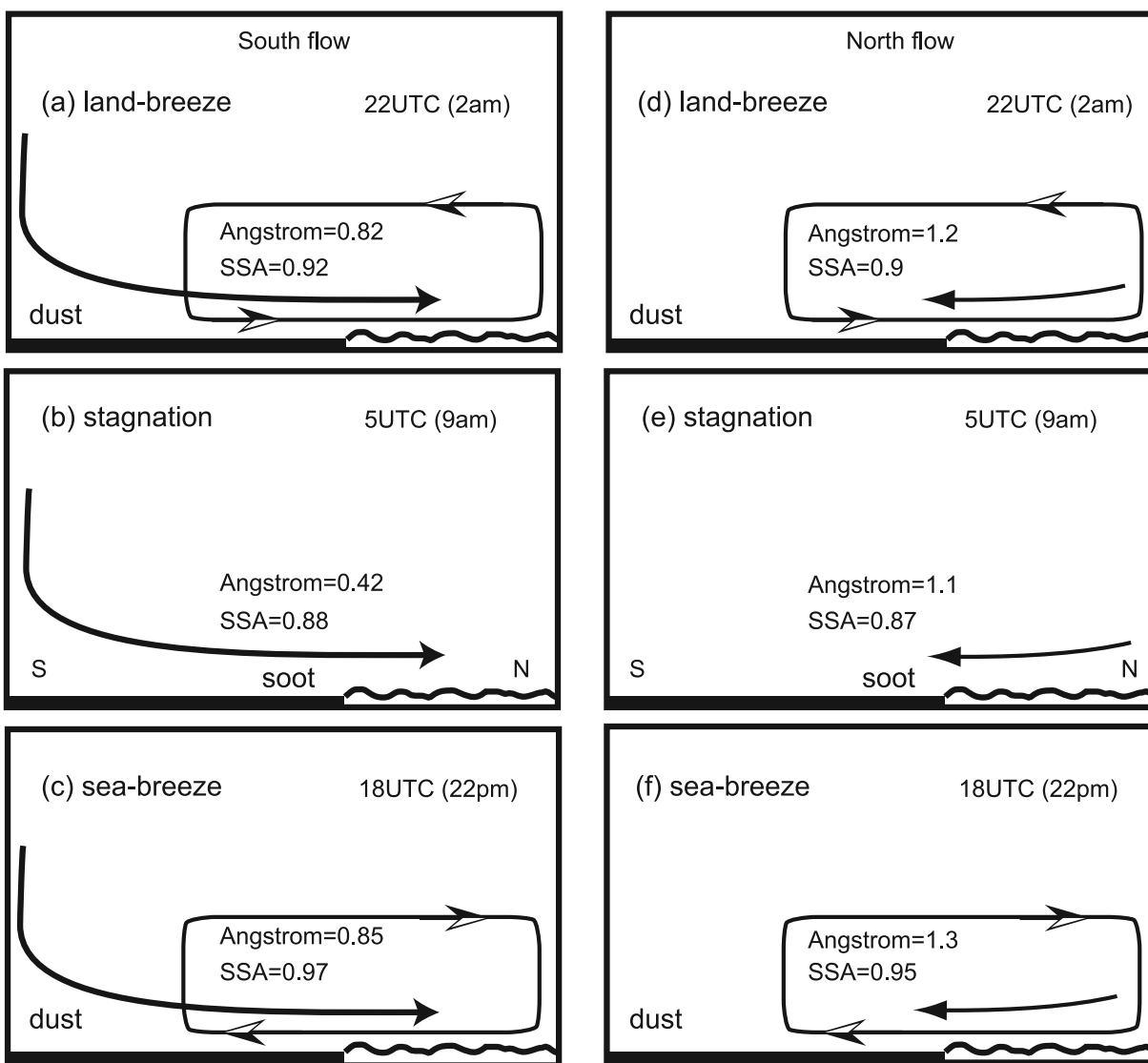
Figure 14. A simplified diagrammatic representation of the interaction between the synoptic-scale airflow and local sea and land breeze circulations. (a, b, c) Southern flows and (d, e, f) northern cases.

model provide means to identify the source region. We distinguish two main synoptic-scale flows corresponding to 80% of all cases. The "north flow" carries smaller particles with Ångstrom coefficient greater than 1 and mean value of 1.22. Flow from south brings larger particles with mean value of the Ångstrom exponent of 0.68. Aerosols for the "north flow" case are more absorptive than aerosol for the "south flow" case. Mean value of the absorption coefficient at 550 nm for the northern flow is 14.9 ± 1.3 Mm^{-1} and for the southern flow is 10.9 ± 0.9 Mm^{-1}. Sea breeze influence on the optical properties of aerosols is greater in the case of the "south flow". Mean values of the absorption coefficient at 550 nm during the sea breeze for the southern flow are almost 2 times less than for northern cases.

References

Alpert, P., and E. Ganor (2001), Sahara mineral dust measurements from TOMS: Comparison to surface observations over the Middle East for the extreme dust storm, March 14–17, 1998, *J. Geophys. Res.*, *106*, 18,275–18,286.

Anderson, T. L., et al. (1996), Performance characteristics of a high-sensitivity, three-wavelength, total scatter/backscatter nephelometer, *J. Atmos. Oceanic Technol.*, *13*, 967–986.

Arnott, W. P., K. Hamasha, H. Moosmuller, P. J. Sheridan, and J. A. Ogren (2005), Towards aerosol light-absorption measurements with a 7-wavelength aethalometer: Evaluation with a photoacoustic instrument and 3-wavelength nephelometer, *Aerosol Sci. Technol.*, *39*, 17–29.

Barnard, J. C., et al. (2005), Measurements of black carbon specific absorption in the Mexico City metropolitan area during the MCMA 2003 field campaign, *Atmos. Chem. Phys. Disc.*, 4083–4113.

Bohren, C. F. (1987), Multiple scattering of light and some of its observable consequences, *Am. J. Phys.*, *55*, 524–533.

Bond, T. C., and R. W. Bergstrom (2006), Light absorption by carbonaceous particles: An investigative review, *Aerosol Sci. Technol.*, *40*, 20–67.

Draxler, R. R., and D. G. Hess (1998), An overview of the Hysplit_4 modeling system for trajectories, dispersion, and deposition, *Austral. Meteorol. Mag.*, *47*, 295–308.

Draxler, R. R., J. T. McQueen, and B. J. B. Stunder (1994), An evaluation of air pollutant exposures due to the 1991 Kuwait oil fires using a Lagrangian model, *Atmos. Environ.*, *28*, 2197–2210.

Dubovik, O., B. Holben, T. F. Eck, A. Smirnov, Y. J. Kaufman, M. D. King, D. Tanré, and I. Slutsker (2002), Variability of absorption and optical properties of key aerosol types observed in worldwide locations, *J. Atmos. Sci.*, *59*, 590–608.

Fialho, P., A. D. A. Hansen, and R. E. Honrath (2005), Absorption coefficients by aerosols in remote areas: a new approach to decouple dust and black carbon absorption coefficients using seven-wavelength aethalometer data, *J. Aerosol Sci.*, *36*, 267–282.

Hansen, A. D. A., H. Rosen, and T. Novakov (1996), The aethalometer: An instrument for the real-time measurement of optical-absorption by aerosol-particles, *Sci. Total Environ.*, *36*, 191–196.

Haywood, J. M., P. N. Francis, M. D. Glew, and J. P. Taylor (2001), Optical properties and direct radiative effect of Saharan dust: A case study of two Saharan dust outbreaks using aircraft data, *J. Geophys. Res.*, *106*, 18,417–18,430.

Haywood, J., P. Francis, S. Osborne, M. Glew, N. Loeb, E. Highwood, D. Tanré, G. Myhre, P. Formenti, and E. Hirst (2003), Radiative properties and direct radiative effect of Saharan dust measured by the C-130 aircraft during SHADE: 1. Solar spectrum, *J. Geophys. Res.*, *108*(D18), 8577, doi:10.1029/2002JD002687.

Heintzenberg, J., and R. J. Charlson (1996), Design and applications of the integrating nephelometer: A review, *J. Atmos. Oceanic Technol.*, *13*, 987–1000.

Hess, M., P. Koepke, and I. Schult (1998), Optical properties of aerosols and clouds: The software package OPAC, *Bull. Am. Meteorol. Soc.*, *79*, 831–844.

Hobbs, P. V., and L. F. Radke (1992), Airborne studies of the smoke from the Kuwait oil fires, *Science*, *256*, 987–991.

Kalashnikova, O. V., R. Kahn, I. N. Sokolik, and W.-H. Li (2005), Ability of multiangle remote sensing observations to identify and distinguish mineral dust types: Optical models and retrievals of optically thick plumes, *J. Geophys. Res.*, *110*, D18S14, doi:10.1029/2004JD004550.

Langner, J., H. Rodhe, P. J. Crutzen, and P. Zimmerman (1992), Anthropogenic influence on the distribution of tropospheric sulphate aerosol, *Nature*, *359*, 712–716.

Léon, J.-F., and M. Legrand (2003), Mineral dust sources in the surroundings of the north Indian Ocean, *Geophys. Res. Lett.*, *30*(6), 1309, doi:10.1029/2002GL016690.

Li, F., and V. Ramanathan (2002), Winter to summer monsoon variation of aerosol optical depth over the tropical Indian Ocean, *J. Geophys. Res.*, *107*(D16), 4284, doi:10.1029/2001JD000949.

Miller, S. T. K., B. D. Keim, R. W. Talbot, and H. Mao (2003), Sea breeze: Structure, forecasting, and impacts, *Rev. Geophys.*, *41*(3), 1011, doi:10.1029/2003RG000124.

Nakajima, T., T. Hayasaka, A. Higurashi, G. Hashida, N. Moharram-Nejad, Y. Najafi, and H. Valavi (1996), Aerosol optical properties in the Iranian region obtained by ground-based solar radiation measurements in the summer of 1991, *J. Appl. Meteorol.*, *35*, 1265–1278.

Petzold, A., et al. (1997), The dependence of the specific attenuation cross-section on black carbon mass fraction and particle size, *Atmos. Environ.*, *31*, 661–672.

Reid, J. S., et al. (2003), Analysis of measurements of Saharan dust by airborne and ground-based remote sensing methods during the Puerto Rico Dust Experiment (PRIDE), *J. Geophys. Res.*, *108*(D19), 8586, doi:10.1029/2002JD002493.

Smirnov, A., B. N. Holben, O. Dubovik, N. T. O'Neill, T. F. Eck, D. L. Westphal, A. K. Goroch, C. Pietras, and I. Slutsker (2002), Atmospheric aerosol optical properties in the Persian Gulf, *J. Atmos. Sci.*, *59*, 620–634.

Tanré, D., J. Haywood, J. Pelon, J. F. Léon, B. Chatenet, P. Formenti, P. Francis, P. Goloub, E. J. Highwood, and G. Myhre (2003), Measurement and modeling of the Saharan dust radiative impact: Overview of the Saharan Dust Experiment (SHADE), *J. Geophys. Res.*, *108*(D18), 8574, doi:10.1029/2002JD003273.

Weingartner, E., H. Saathoff, M. Schnaiter, N. Streit, B. Bitnar, and U. Baltensperger (2003), Absorption of light by soot particles: Determination of the absorption coefficient by means of aethalometers, *J. Aerosol Sci.*, *34*, 1445–1463.

Zhu, M., and B. W. Atkinson (2004), Observed and modelled climatology of the land-sea breeze circulation over the Persian Gulf, *Int. J. Climatol.*, *24*, 883–905.

————————————
P. J. Flatau, Scripps Institution of Oceanography, University of California San Diego, San Diego, CA 92093-0221, USA.

K. M. Markowicz and M. L. Witek, Institute of Geophysics, Warsaw University, ul. Pasteura 7, 02-03 Warszawa, Poland.

E. A. Reid and J. S. Reid, Naval Research Laboratory, Marine Meteorology Division, 7 Grace Hopper Avenue, Monterey, CA 93943-5502, USA.

J. Remiszewska, Institute of Geophysics, Polish Academy of Sciences, ul. Ksiecia Janusza 64, 01-452 Warszawa, Poland. (jrem@igf.fuw.edu.pl)